Diachronic analysis of land use and land surface temperature in the city of Dakar over the last 30 years

Source: Think Tank “INTERFACE” of the Cheikh Anta Diop University of Dakar (UCAD) on climate finance

Year: March 2025

Table of Contents

List of figures

List of tables

This report was developed as part of the UNI-LEAD project, which aims to strengthen the capacity of universities in the LDC Universities Consortium on Climate Change to provide technical advice and services to their governments for greater access to climate finance. This project is funded by the Global Environment Facility (GEF), implemented by the United Nations Environment Programme (UNEP), and executed by START International in partnership with Climate Analytics, Inc. Prepared by the Senegal Think Tank in collaboration with its partners listed in the table below, this document is accompanied by a policy brief and a project idea proposal for submission to nationally accredited institutions.

First and last name	**Role(s)**	**Institution**
Anastasie MENDY	Leader of the Sustainable City Working Group, responsible for diachronic studies and the bibliographic review	FLSH/UCAD
Sidia BADIANE	Responsible for diachronic studies and bibliographic review	FLSH/UCAD
Awa NIANG	Responsible for diachronic studies and bibliographic review	FLSH/UCAD
Mbayang THIAM	Responsible for diachronic studies and bibliographic review	Institute of Territorial Governance (IGT)/UCAD
Elhadji Mamadou SONKO	Responsible for diachronic studies and bibliographic review, production of project ideas	Institute of Environmental Sciences (IST)/UCAD
Mamoudou DEME	Responsible for diachronic studies and bibliographic review	FLSH/UCAD
Demba NDAO NIANG	Responsible for aerosol studies and bibliographic review	ESP/UCAD
Malick Mbow	Responsible for diachronic studies and bibliographic review	FLSH/UCAD
Abdoulaye SYLLA	Responsible for validating themes and project sheets	Dakar City Hall
	Responsible for validating themes and	DiREC/METE

Laurice FAYE	project sheets	
Ameth BA	Responsible for validating themes and project sheets	Green Spaces Department
Aissatou SALL	Responsible for validating themes and project sheets, capacity building	CSE

This group was established following several discussions between researchers, public and private stakeholders. Professor Anastasie Mendy, head of the Geography Department at UCAD, is the leader of this group, composed of 14 people, including 5 women. The group also includes several young researchers (doctoral and postdoctoral students).

Coordination:

Prof. Amadou Gueye

Dr. Ibrahima Camara

I) INTRODUCTION

Urbanization poses major problems, including the alteration of land surface conditions leading to a changed thermal climate that makes cities warmer than surrounding rural areas(ME Awuh, PO Japhets, MC Officha, AO Okolie, & IC Enete, 2019). Changes in land use and cover (LUC) in response to human activities over time lead to several environmental consequences at multiple scales (e.g., global, regional, and local), such as changes in energy balance and land surface temperature (LST).(Mirza & Sajjadb, 2022).

LST is the result of how Earth's surfaces interact with the atmosphere, producing heat that affects humans. It is influenced by meteorological aspects such as solar radiation, wind speed, and surface properties. Urban heat island (UHI) is a phenomenon in which temperatures are higher in urban areas compared to surrounding rural or natural areas. UHI and elevated LST are mainly caused by human activities and built environments, presenting a clear interconnection (Jianga & Tiana, 2023).

Several authors have recognized that the integration of LST/LU remote sensing and statistical tools can provide spatially continuous data across an entire city or region, allowing visualization of spatial relationships between temperature patterns and land uses, including infrastructural features (ME Awuh, PO Japhets, MC Officha, AO Okolie, & IC Enete, 2019). Of theStatistical and comparative analyses can be performed to examine the causality of the association between LST and some standardized land use and land cover indices such as the Normalized Difference Vegetation Index (NDVI), the Normalized Difference Built-Up Index (NDBI), and the Normalized Difference Water Index (NDWI).

The city of Dakar has experienced a significant influx of people over the past three decades. This population increase has promoted rapid urbanization to accommodate this growing population. Given that urbanization is generally associated with landscape dynamics, this study attempts to answer the following two research questions: (1) How have land cover classes changed over the past three decades across the city of Dakar? (2) How has the city's land surface temperature varied in relation to land cover changes.

II) Materials and methods

II.1) Study area

The city of Dakar is located in the extreme west of the Cape Verde Peninsula, on the edge of the Atlantic Ocean. It covers an area of approximately 83 km², with latitudes ranging from 14°40′ to 14°46′ N and longitudes from −17°32′ to −17°24′ W. It has 18 municipalities and a total population of 1,278,469 inhabitants in 2023 according to ANSD (RGPH-5,2024).

It is the political and economic capital of Senegal, with commercial, industrial, and port activities. The city is home to numerous businesses and multinationals, as well as public services, financial, and diplomatic institutions.

Dakar has a tropical arid climate, with a long dry season from November to May and a rainy season from July to early October. Due to its location, the climate is milder than the rest of Senegal. During the dry season, cool oceanic winds blow from the north, and mist can sometimes form. In the hot, humid, and rainy season, on the other hand, the wind is weaker and variable in direction (Source:(Climates and Travel, nd)

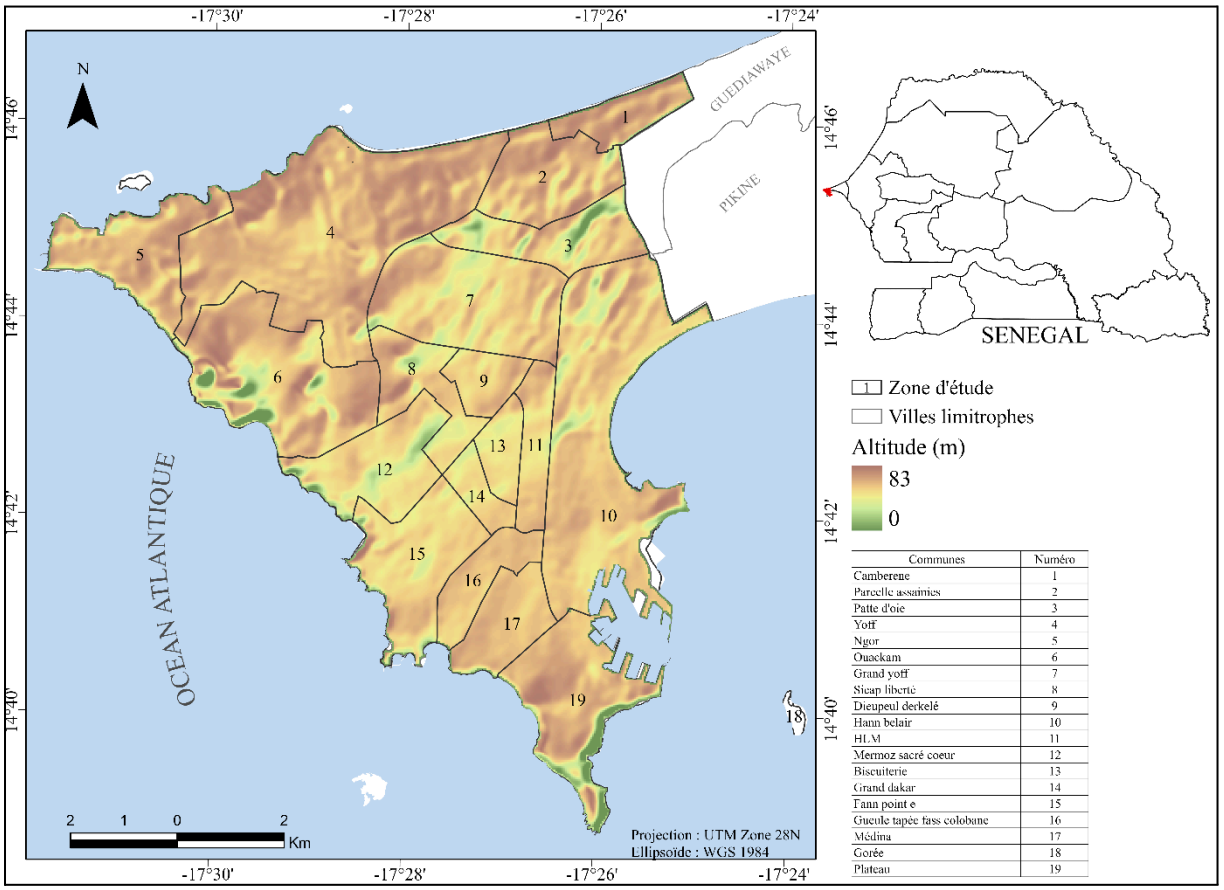

Communes	Numéro
Camberene	1
Parcelle assainies	2
Patte d'oie	3
Yoff	4
Ngor	5
Ouackam	6
Grand yoff	7
Sicap liberté	8
Dieupeul derkelé	9
Hann belair	10
HLM	11
Mermoz sacré coeur	12
Biscuiterie	13
Grand dakar	14
Fann point e	15
Gueule tapée fass colobane	16
Médina	17
Gorée	18
Plateau	19

II.1.1.1) Figure 1: Location map of the city of Dakar

II.2) Materials

To carry out this study, a methodological approach based on the analysis of satellite data and geographic information systems (GIS) was adopted, integrating specific tools for the spatio-temporal analysis of land cover and land surface temperature. The diagram below shows the flowchart of the general methodology of the study.

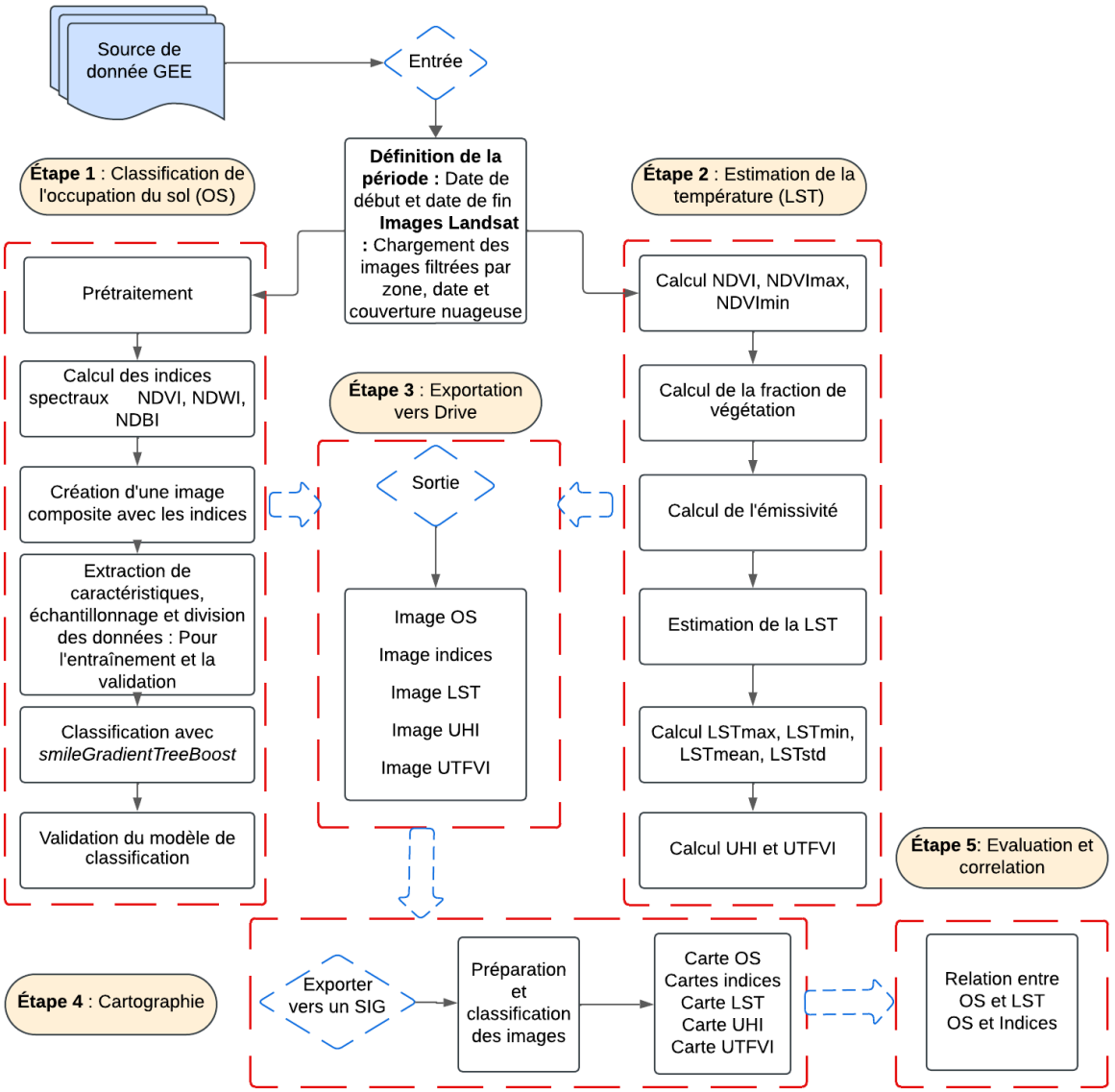

II.2.1.1) Figure 2: Flowchart of the general methodology

II.2.2) Tools

The geospatial processing and analysis tools and software used in this study were essential, providing advanced functionalities for satellite image processing, mapping and data integration, thus enabling an in-depth analysis of the observed phenomena.

II.2.2.1) Table 1: Presentation of the different tools and software used

Software & Tools	Main features	Uses
Google Earth Engine (GEE)	Large-scale geospatial data analysis and processing. Access to a vast library of satellite images and geospatial data. Scripting language for data analysis.	Time series analysis for LST and OS. Calculation of indices (NDVI, NDBI, NDWI.).
QGIS	Open-source GIS software for visualizing, processing, and analyzing geospatial data. Support for numerous file formats and plugins for advanced analytics.	Mapping and visualization of OS and LST data. Merging and transformation of geospatial layers
ArcGIS Pro & ArcMap	Advanced tools for analyzing and visualizing geospatial data. Geoprocessing, spatial analysis, and modeling. User-friendly interface with extensive mapping capabilities.	Detailed spatial analysis of OS and LST data. Creation of thematic maps and geospatial reports.
Excel	Data management and analysis in spreadsheet form. Statistical calculation and data visualization in graphic form.	Statistical analysis of LST results. Creation of graphs and summary tables for OS data.
R/RStudio	A free, open-source, cross-platform development environment for R, a programming language used for data processing and statistical analysis.	Correlation analysis between LST and spectral indices

II.2.3) Data used

Landsat 5 TM for 1986, Landsat 7 TM 2000 and Landsat 8 OLI 2013 and 2023 were selected due to their availability and spatial resolution for multispectral and thermal bands, which favors precise localization of different land uses and LST monitoring. All images were acquired over the period of one year with the extraction of the median image by synthesis.

II.2.3.1) Table 2: Presentation of Landsat data used

Satellites	Sensors	Years	Projection	Spatial resolution	Number of bands
Landsat 5	TM	1986	UTM Zone 28 N	30 m	7
Landsat 7	ETM+	2000	UTM Zone 28 N	30 m	7
Landsat 8	OLI	2013 & 2023	UTM Zone 28 N	30 m	11

II.3) Methods

The methods used consisted of image preprocessing and classification, calculation of land cover indices (NDVI, NDBI, NDWI), calculation of the urban heat island and the determination of the Land Surface Temperature (LST)using thermal bands for the entire Landsat data set.

The methodology used to calculate LST is based on Landsat sensor data. The TM sensor was used for Landsat 5 images, ETM+ for Landsat 7, and the OLI sensor was used for Landsat 8 images.

The different steps that were followed to extract the ground surface temperature from the thermal bands of the LANDSAT images are as follows:

II.3.1) Conversion of DN (Digital number) into reflectance and image filtering

DN conversion and data filtering are essential steps to ensure the accuracy of measurements from satellite images.

Here is a description of these steps that was carried out on the Google Earth Engine platform:

II.3.1.1) Converting DN (Digital Number) to Reflectance

Digital number **(DN)**: It is a raw digital value recorded by a satellite sensor. It represents the intensity of the signal received by the sensor for a given spectral band. DNs are not directly comparable between different images or even between different bands of the same image.

Reflectance: It is the proportion of incident light that is reflected by a surface. It is expressed as a percentage and is a more meaningful physical measurement than DN, because it allows for comparison of different surfaces and analysis of material properties.

The purpose of converting Digital Numbers (DN) values to reflectance is to make satellite data comparable and usable for quantitative analyses. It is applied to both optical and thermal bands using specific scaling factors. For optical bands (SR_B. bands), a correction factor is applied: SR_B.* = SR_B. * 0.0000275 + (-0.2). For thermal bands (ST_B.*), the correction is performed with the formula ST_B.* = ST_B. * 0.00341802 + 149.0. These coefficients are used to convert raw digital values into physically meaningful values (reflectance).

II.3.1.2) Data filtering

Data filtering is important to remove pixels affected by clouds, cloud shadows, or other anomalies that could introduce errors into calculations. By removing these unwanted pixels, the quality of the images used for analysis can be significantly improved.

This step involves identifying and masking pixels affected by clouds using algorithms like QA_PIXEL to detect clouds and their shadows in Landsat images. The mask is applied to keep only clear (non-cloudy) and reliable pixels for further calculations.

II.3.2) Calculation of NDVI, vegetation fraction and emissivity

II.3.2.1) Calculation of NDVI

The Normalized Difference Vegetation Index (NDVI) is a vegetation index widely used in remote sensing and environmental science. It quantifies the presence and health of vegetation based on the reflectance of visible and near-infrared light. NDVI values typically range from -1 to 1, with higher values indicating healthier or denser vegetation.

NDVI is calculated using the following formula:

$$NDVI = \frac{PIR - Rouge}{PIR + Rouge}$$

NIR (near infrared) is the reflectance in the near infrared portion of the electromagnetic spectrum.

Red is the reflectance in the red part of the electromagnetic spectrum.

After calculating the NDVI, we proceeded to determine its minimum and maximum values which will be used to estimate the plant fraction.

II.3.2.2) Estimation of the vegetation fraction (VF)

Vegetation fraction (VF) is a metric used to quantify the relative abundance of vegetation in a specified area by analyzing Normalized Difference Vegetation Index (NDVI) values. It is defined as the ratio of the vertical projection area of vegetation (containing leaves, stems, and branches) on the ground to the total vegetation area. It provides valuable information on land cover and ecosystem health, with higher VF values indicating greater vegetation presence and vice versa.

FV is calculated using the following formula:

$$FV = \left(\frac{NDVI - NDVImin}{NDVImax - NDVImin}\right)^2$$

NDVImin represents the minimum NDVI and NDVImax represents the maximum NDVI

II.3.2.3) Emissivity estimation (ε)

It is calculated based on the PV, reflecting how efficiently a surface emits thermal radiation. Emissivity values close to 1.0 are typical of natural surfaces such as soil and vegetation, while lower values are often associated with bodies of water or urban areas. ε is calculated using the formula below:

$$\varepsilon = 0,004 * FV + 0,986$$

The coefficient 0.004 represents the variation in emissivity due to vegetation and 0.986 represents the basic emissivity for other surfaces.

II.3.3) Estimation of land surface temperature (LST)

LST, expressed in °C, was derived from the thermal bands of Landsat 5 and 7 TM (band 6) and Landsat 8 OLI (band 10). Areas with high temperatures have higher LST values and vice versa. LST is obtained using the formula below (Pal & Ziaul, 2017),(Niladri, Prolay, Subhasish, & Ranajit, 2021):

$$LST = \left(\frac{BT}{1+\{\left(\frac{\gamma * BT}{\rho}\right) * ln\varepsilon\}}\right) - 273,15$$

Where BT is the Landsat thermal band, is the wavelength of the emitted radiance (11.5μm)γ(Mwangi, Faith, & Peter, 2018),$\rho = \frac{h*c}{\sigma} = 1,438 * 10 - 2mK$(σ = Boltzmann constant ($1.38 * 10^{-23}$ J/K), h = Planck's constant ($6.626 * 10^{-34}$ J s), and c = speed of light (2.998 × 10 8 m/s)) (Pal & Ziaul, 2017).

II.3.4) Estimation of the urban heat island index (UHI)

An urban heat island is the name given to describe the characteristic warmth of the atmosphere and surfaces of cities (urban areas) relative to their surroundings (non-urbanized). Heat islands are caused by urbanization, when buildings, roads, and paved surfaces store heat during the day and then slowly release it during the evening, keeping urban areas warmer than surrounding areas (Mwangi, Karanja, & Kamau, 2018). Areas with higher infrastructure densities have much higher UHI values and poor ecological condition.

UHI is determined according to the following formula:

$$UHI = \frac{LST - LSTmean}{LSTstd}$$

Where LSTmean represents the mean surface temperature and LSTstd the standard deviation of the surface temperature.

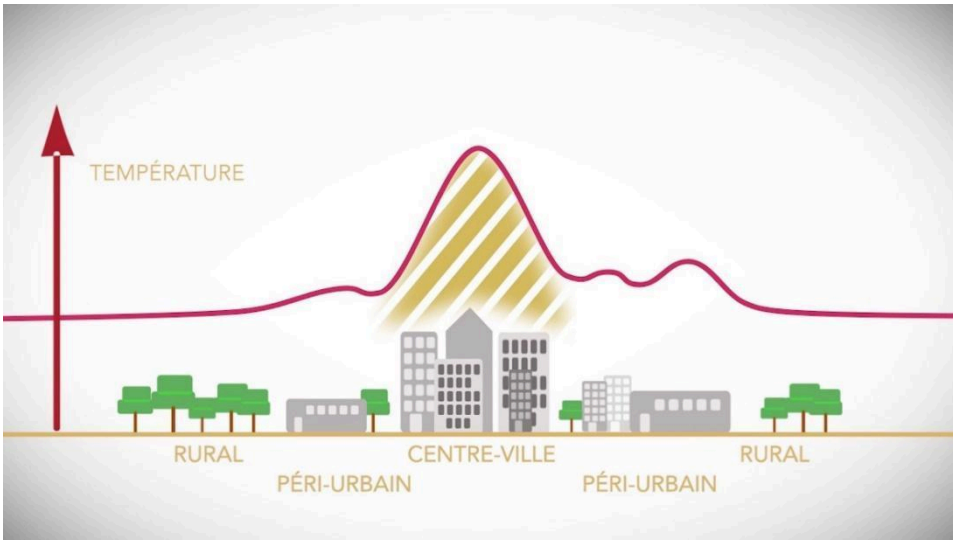

II.3.4.1) Figure 3: Illustrative diagram of the heat island

II.3.5) Estimation of the Urban Thermal Field Variation Index (UTFVI)

The Urban Thermal Field Variation Index is a quantitative measure that expands on the idea of urban heat island intensity. It examines differences in LST within an urban area. A high UTFVI score correlates with decreased biodiversity, highlights the importance of an exacerbated urban heat island phenomenon, and an increase in extreme urban temperatures. This discrepancy in temperature distribution is a defining characteristic of a surface urban heat island (SUHI) effect. Various studies have used the equation given by (Yong et al., 2006) to extract UTFVI from LST data (Gajani, 2024).

$$UTFVI = \frac{Ts - Tmean}{Tmean}$$

Where Ts is the LST of the pixel and Tmean means the average LST of the study area. According to the variations, we classified the UTFVI into six distinct categories: none, weak, medium, strong, stronger and strongest.

II.3.6) Extraction of other spectral indices

Spectral indices are used to highlight specific features or phenomena in remote sensing images. We create spectral indices by transforming spectral data using ratios between bands to reduce the data into meaningful information. Features that can be extracted using spectral indices range from vegetation, buildings, wet surfaces, among many others.

II.3.6.1) Normalized Difference Water Index (NDWI)

The Normalized Difference Water Index (NDWI) is used to detect open water basins in satellite imagery: the water body "stands out" from the soil and vegetation. It was proposed by McFeeters in 1996. Today, it is mainly used to detect and monitor small changes in water content in water basins. It uses the advantages of NIR (near infrared) and GREEN (visible green). It is obtained according to the following formula:

$$NDWI = \frac{GREEN-NIR}{GREEN+NIR}$$

GREEN is the green band and NIR is the near infrared band.

II.3.6.2) Normalized Difference Building Index (NDBI)

Normalized Difference Building Index (NDBI) describes the building density of any geographical area. NDBI is a ratio of shortwave infrared (SWIR) to near infrared (NIR). NDBI was calculated (according to Pal & Ziaul, 2017) by:

$$NDBI = \frac{SWIR-NIR}{SWIR+NIR}$$

SWIR is the short infrared band and NIR is the infrared band.

II.3.6.3) Bare Soil Index (BSI)

The Bare Soil Index (BSI) is a numerical indicator that combines blue, red, near infrared, and shortwave infrared spectral bands to capture soil variations. BSI can be used in many remote sensing applications, such as soil mapping, etc. It is calculated using the following formula:

$$BSI = \frac{(RED+SWIR)+(-1*(NIR+BLUE))}{(RED+SWIR)+(NIR+BLUE)}$$

RED is the red band, BLUE is the blue band

II.3.7) Land use and occupation classification (OS)

To generate the OS maps, the supervised image classification technique with method of *smile Gradient Tree Boost* was used on the Google Earth Engine platform.

A large number of training points were collected through visual interpretation and color combination from the entire imagery. A total of 2,730 points were collected over the four years of the study, distributed as follows:

- 1885 used for model calibration, i.e. 70% of the points of training
- 845 used for model validation, i.e. 30% of the points of training

The table below gives the repair of samples for each year

II.3.7.1) Table 3:Distribution of sample points by year

Years	Sample points		
	Calibrations	Validations	Total
1986	564	235	799
2000	491	229	720
2013	465	244	709

2023	365	137	502
TOTALS	1885	845	2730

For this purpose, four classes have been defined and distributed as follows:

- Built: it covers buildings for residential and commercial purposes, roads, airports, port
- Vegetation: these areas include fields, green spaces, trees, natural vegetation,
- wet vegetation
- Water: This refers to areas covered by the ocean, lakes, stagnant waters
- Bare ground: these are empty spaces without built structures or any land use

The diagram below shows the entire supervised classification process:

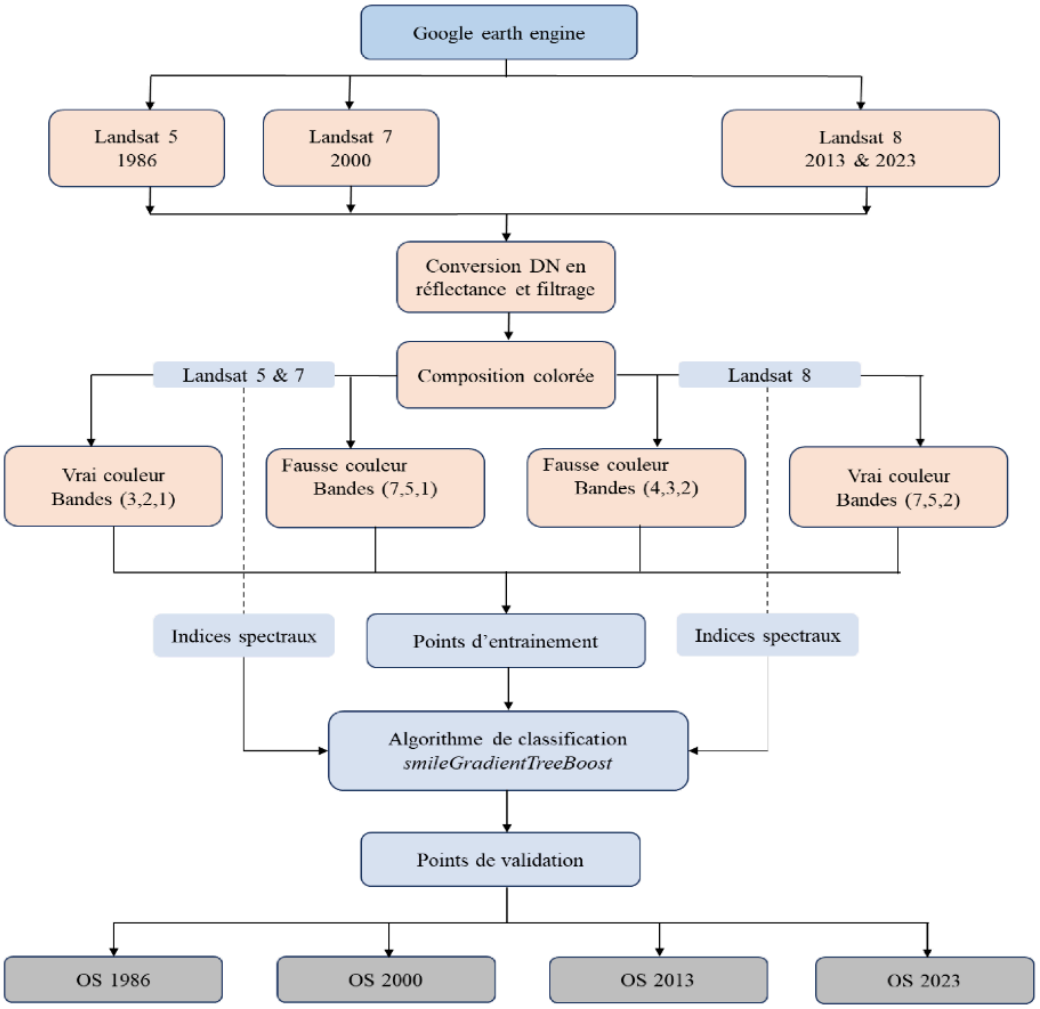

II.3.7.2) Figure 4: Flowchart of land use and land cover classification

II.3.8) Evaluation of the accuracy of classification models

Classification accuracy was assessed using the kappa coefficient (K) and overall accuracy (OA) was obtained using a confusion matrix which is a widely used method for classification accuracy (Ullah, Fan, & Liu, 2019). OA is expressed as the percentage of the number of correctly classified pixels divided by the total number of pixels. To assess the discrepancies between the expected classification accuracy and the actual classification accuracy, the Kappa statistical index was used. In this study, 30% of the collected points were used to assess the classification accuracy for each image.

The mathematical equations used to estimate the previously mentioned statistics are described below:

- $OA = \frac{\sum_{i=1}^{r} nij}{N}$
- $K = N \sum_{i=1}^{n} nii - \sum_{i=1}^{r} \frac{col \ \ lig}{N^2} - \sum_{i=1}^{r} col \ \ lig$

nii is the number of pixels correctly classified into a category; N is the total number of pixels in the confusion matrix; r is the number of rows; and nicol and nlig are the total of columns (reference data) and rows (predicted classes).

II.3.9) Statistical analysis method

Statistical analysis was performed using R/R studio software. The different spectral indices were combined with LST to determine their relationship with these different parameters.

III) Outcomes

III.1) Land use analysis (LU)

Considering the interest of the study and the dominant LU, four (04) classes were generated. Few other LU classes can be generated, but their proportion is too low and is not even reflected clearly. For this, these undefined pixels were incorporated into the neighboring classes within the system. The final result gives an image that shows the change in land use between 1986, 2000, 2013 and 2023 (fig. 6).

The graph presents a complete data set on areas subject to different LU (Fig. 7).

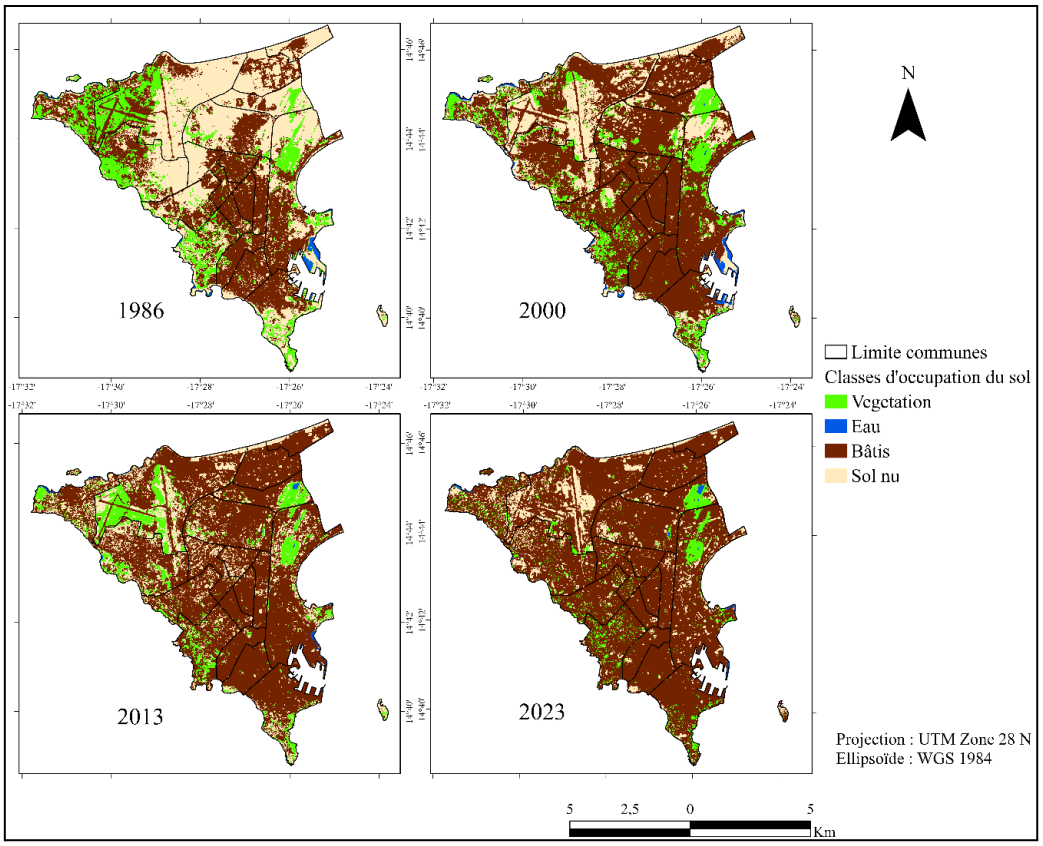

III.1.1.1) Figure 5: Land use map of the city of Dakar from 1986 to 2023

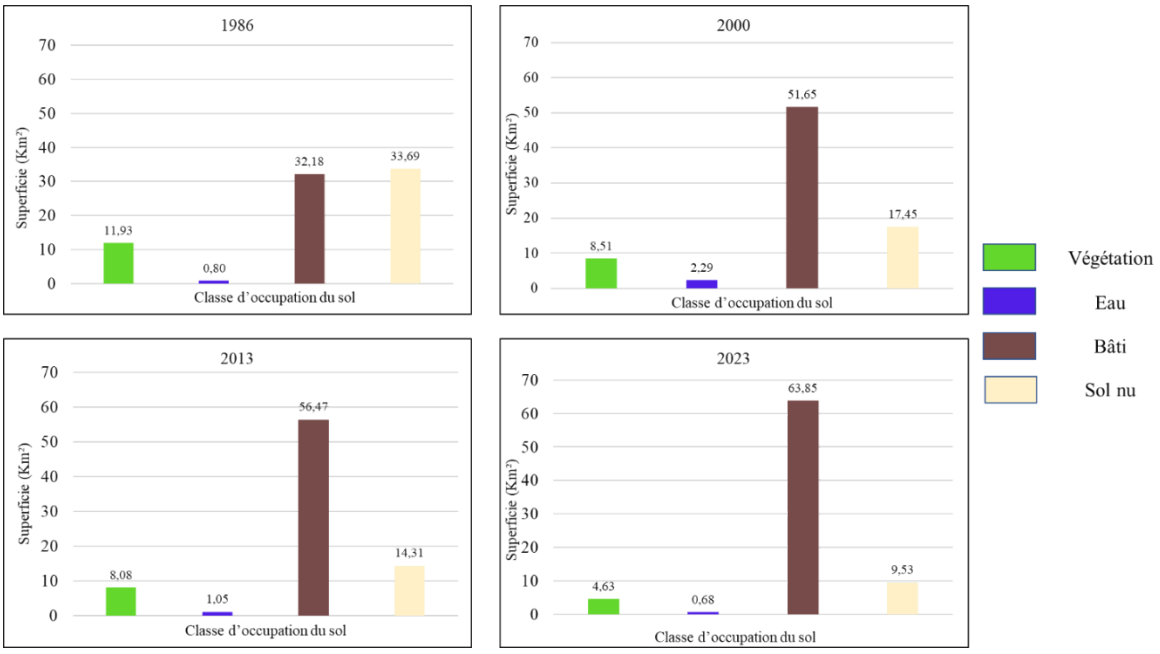

III.1.1.2) Figure 6: Histogram of land use classes from 1986 to 2023

III.2) Assessment of classification accuracy

The basic principle for any accuracy assessment is to compare estimates with reality, and to quantify the difference between the two. In the context of remote sensing-based land cover classifications, "estimates" are the mapped classes for each pixel, and "reality" is the actual land cover in the areas corresponding to each pixel.

The classification accuracy was assessed using the Google Earth Engine platform. To validate the classified maps, the points collected were 565 for the year 1986, 490 for the year 2000, 464 for the year 2013 and 364 for the year 2023. The overall accuracy indicates to what extent the classification results exactly meet our expectations. The overall accuracies of the classified images were respectively 87.9%; 77.7%; 86.4% and 91.9% for the years 1986, 2000, 2013, 2023 with Kappa coefficients of 0.8; 0.656; 0.806 and 0.807. It should be noted that the Kappa coefficient is a measure of the proportional (or percentage) improvement of the classifier compared to a purely random assignment to classes (Pal & Ziaul, 2017) (Table 4).

III.2.1.1) Table 4: Confusion matrices, Kappa coefficients and overall accuracies of the different OS classes

Année		Végétation	Eau	Bâti	Sol nu	Totale	Précision globale	Coefficient Kappa
1986	Végétation	44	0	3	8	55	0,879 (87,9%)	0,8
	Eau	0	12	0	0	12		
	Bâti	3	0	30	7	40		
	Sol nu	7	0	3	118	128		
	Totale	54	12	36	133	235		
2000	Végétation	32	0	6	1	39	0,777 (77,7%)	0,656
	Eau	0	14	1	0	15		
	Bâti	6	0	37	13	56		
	Sol nu	1	1	22	95	119		
	Totale	39	15	66	109	229		
2013	Végétation	42	0	1	2	45	0,864 (86,4%)	0,806
	Eau	1	26	0	0	27		
	Bâti	3	0	57	16	76		
	Sol nu	2	0	8	86	96		
	Totale	48	26	66	104	244		
2023	Végétation	32	0	1	0	33	0,919 (91,9%)	0,887
	Eau	1	13	0	0	14		
	Bâti	1	0	38	2	41		
	Sol nu	0	0	6	43	49		
	Totale	34	13	45	45	137		

III.3) Land surface temperature (LST) mapping of the city of Dakar

The map below (Figure 8) shows the temperature change from 1986 to 2023. In all maps, the bright reddish tone highlights higher temperatures and the bluish tone highlights lower LSTs. A change in temperature was observed over the four years, in 1986 the average land surface temperature was 32.23°C which is somewhat similar to that of 2000 which is around 32.20°C; and the average land surface temperature of 2013 and 2023 are 36.98°C and 37.69°C respectively.

The temporal change in land surface temperature has changed with the rapid change in land use/land cover. From 2000 onwards, the maximum temperature is seen to be concentrated around industrial and residential areas.

The local climate is influenced by the evolution of the OS model. The rate of increase in the impervious surface leads to a change in the LST. In 1986, the area covered by buildings was 32.18 km² and this value almost doubled in 2023 and increased from 63.853 km², thus making the surfaces of the city of Dakar impervious, leading to the gradual variation of the temperature of the earth's surface. Figure 9 shows the variation in temperature over the years. We see that the minimum and maximum temperatures increase over the years. The average temperature also follows this logic. We also note a decrease in the range between extreme temperatures which could be attributed to the change in use and occupancy over the years.

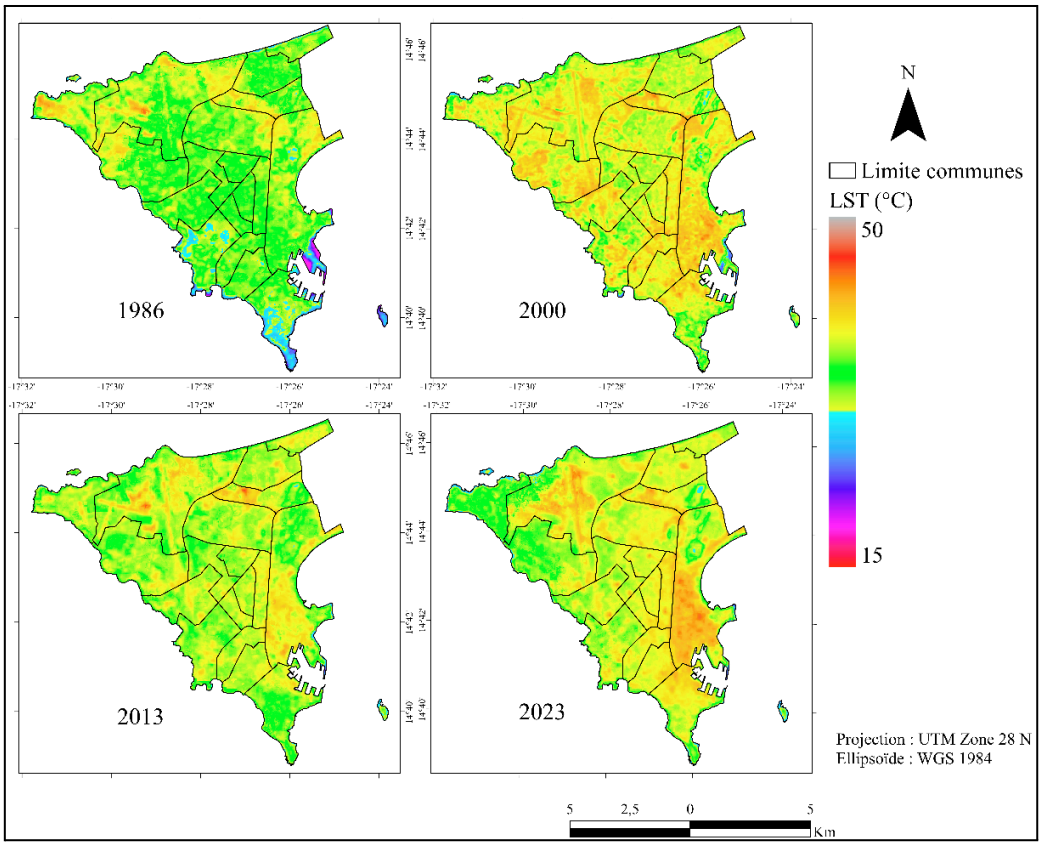

III.3.1.1) Figure 7: Map of LST distribution from 1986 to 2023

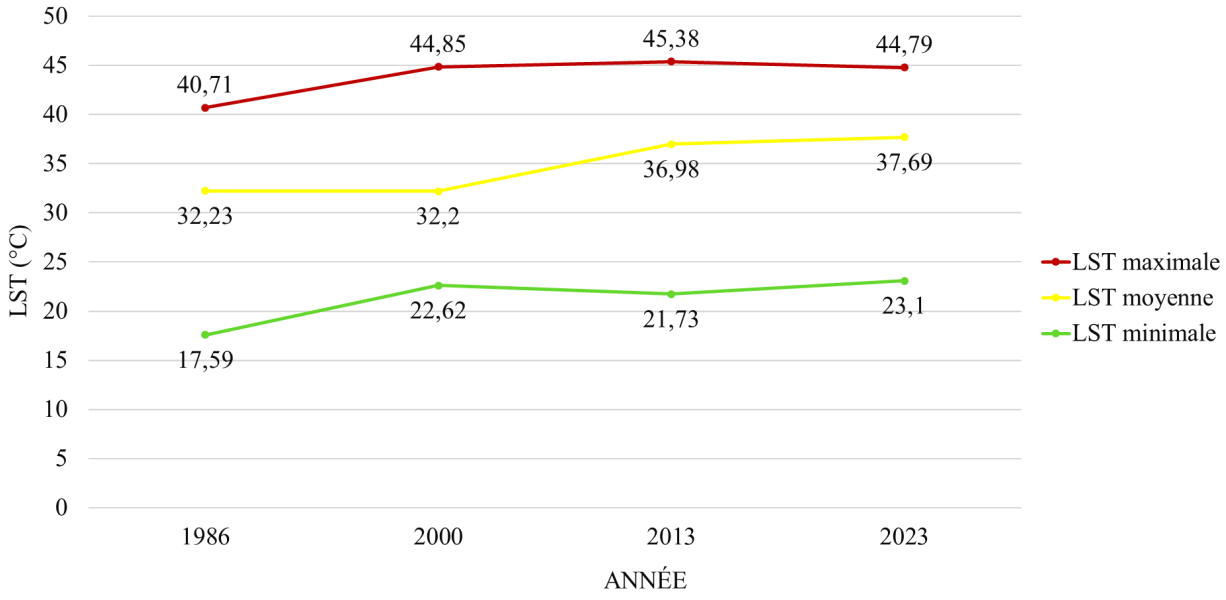

III.3.1.2) Figure 8: Variation of mean, maximum and minimum LST values over the years

III.4) Urban Heat Island (UHI) Analysis

The analysis of the figure allows us to see the variation of the heat island between different years. We observe a general trend in the UHI over the years (Figure 10). The reddest areas characterize the

highest temperatures in urbanized areas compared to the surrounding areas. UHIs are concentrated in the central areas of the city and in the industrial area of the city (municipality no. 10 Hann Bel Air). These are the most urbanized areas in the city and cover almost all industrial activities and road infrastructure. The figure shows us the variation of the UHI for different surface categories over the years.

Figure 11 shows the evolution of the urban heat island over the years. We see that natural spaces such as vegetation and water have the lowest UHI values, thus characterizing their role as a buffer by limiting the evolution of temperature. While in built-up areas, we observe a progressive increase in temperature. And this is the same case for bare soils (Figure 11).

Built-up areas are increasingly concentrating heat. This trend is explained by rapid urbanization, soil impermeability, and the reduction of vegetation and wetlands.

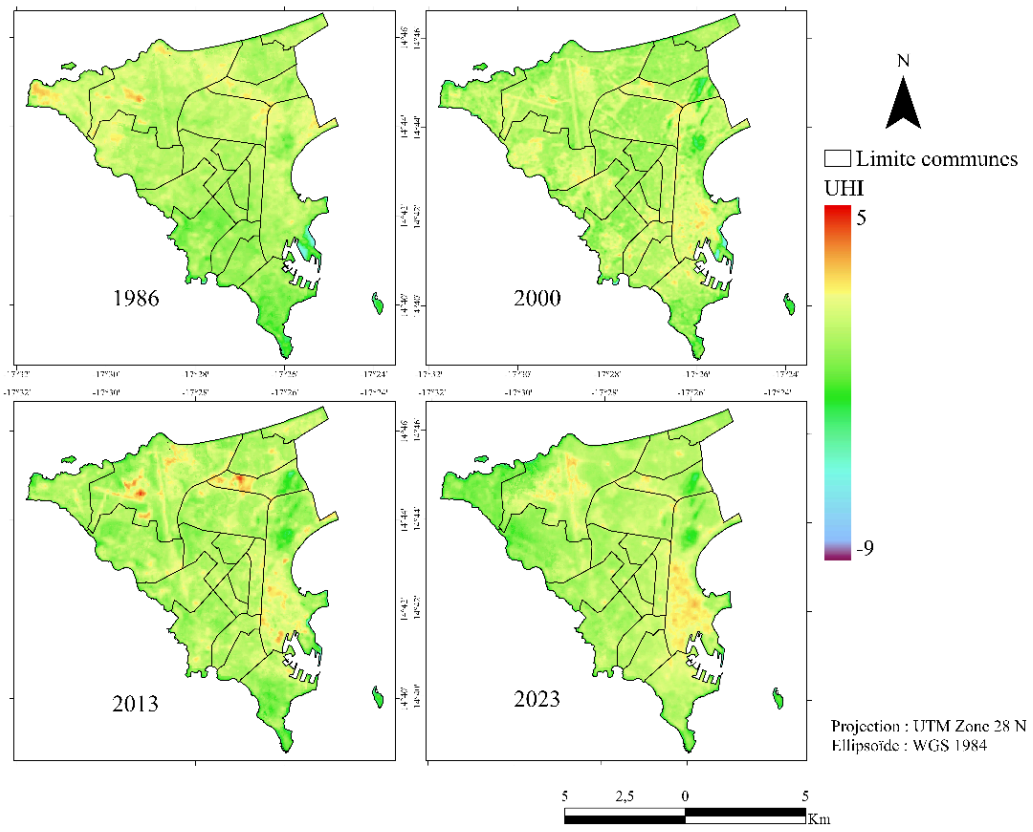

III.4.1.1) Figure 9: Map of UHI distribution over the years

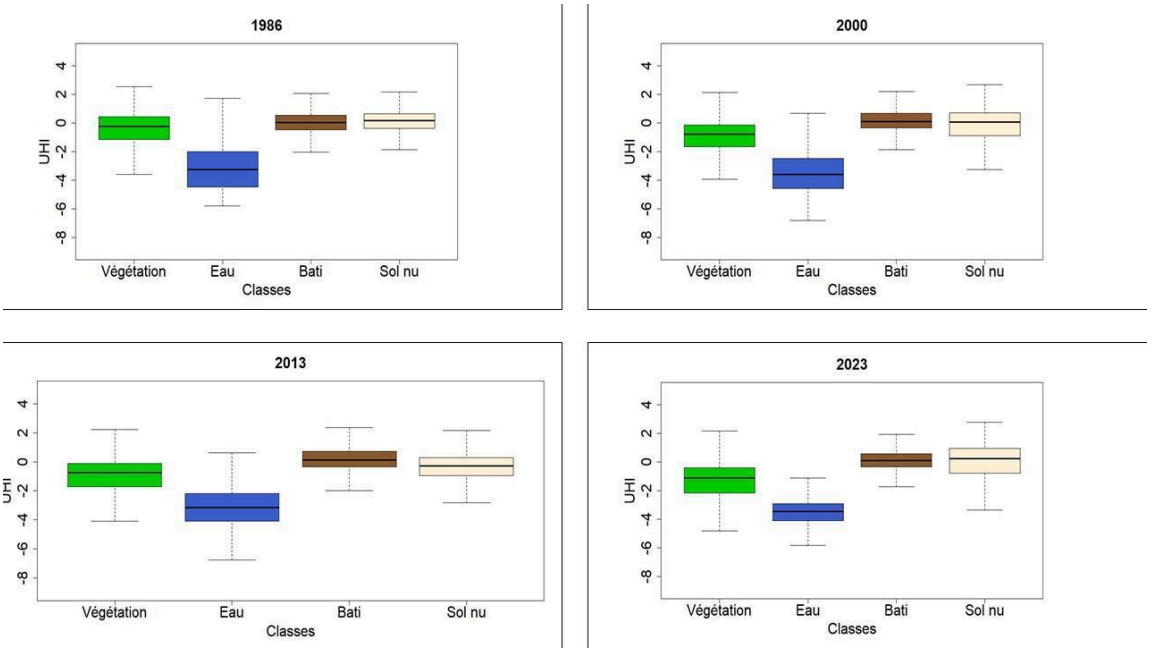

III.4.1.2) Figure 10: Variation of UHI values between different land use classes

III.5) Urban Thermal Field Variation Index (UTFVI)

The UTFVI value was also measured to elucidate the influence of urban heat islands (UHI) on the urban environment in Dakar. It was used in this study to provide a quantitative analysis of the influence of UHI on ecological degradation. In terms of ecological assessment index (Table 5). The figure shows the analysis conducted on UTFVI over the years.

According to the UTFVI value, we found that poor ecological conditions were present on the Northeast side of the map in 1986, almost over the entire area in 2000 and a large part on the Southeast in 2013 and 2023 (Fig. 11). The change in the location of UHI over the years may be due to the changes in OS. According to the scale of UTFVI value (Table 5), a strong UHI was found on the west side of the study area in 2013 and 2023 which corresponds to the industrial zone of Dakar city (Fig. 11).

Table 5: Diagram of the Urban Thermal Field Variance Index (UTFVI) scale. (Source ((Bubun, Siba, The Archivist, Rana, & Mukul, 2024)))

UTFVI value	UHI phenomenon	Ecological Assessment Index
<0.000	None	Excellent
0.000–0.005	Weak	GOOD
0.005–0.010	Medium	Normal
0.010–0.015	Strong	Bad

0.015–0.020	Stronger	Worse
>0.020	The strongest	Worse

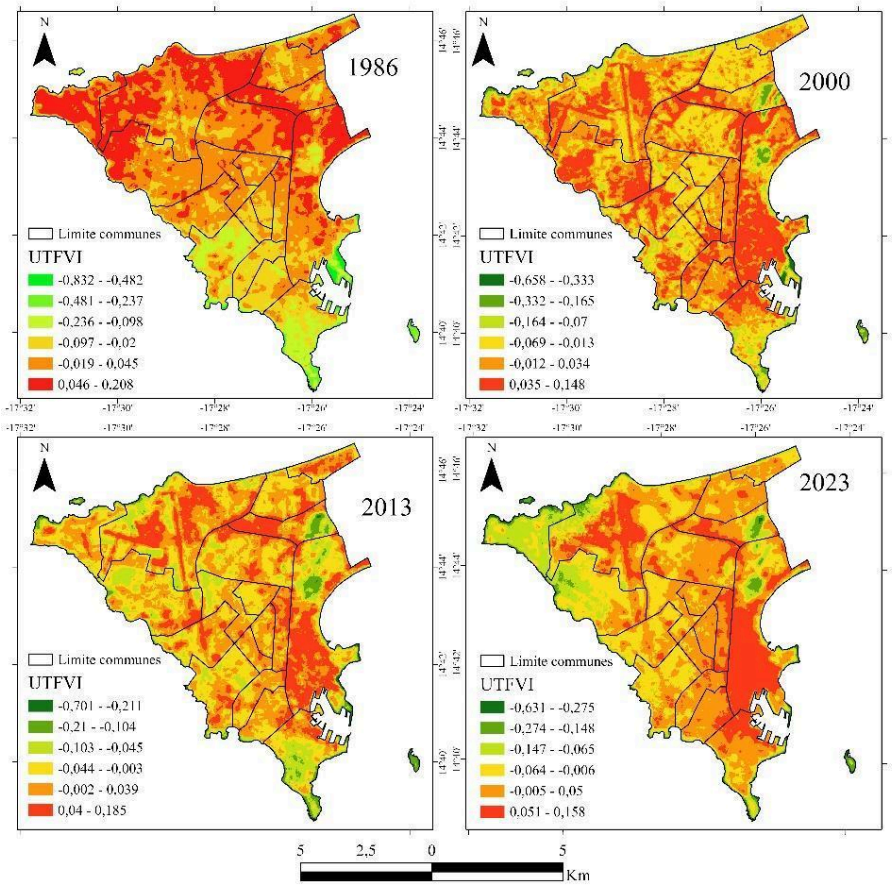

III.5.1.1) Figure 11: Spatial distribution map of UTFVI over the years

III.6) Statistical analysis results

As listed in the methodology section, a statistical analysis was performed to see the different relationships between LST and land cover and land use (LU) classes and between LST and spectral indices.

III.6.1) Variation of LST in different land use classes

Figure 13 shows the variation of LST in different classes in the form of a boxplot. It allows us to see the evolution of the land surface temperature for different soil classes.

We see that the vegetation and bare soil classes always have the lowest average temperatures over the years. Unlike the built-up and bare soil classes, which seem to vary together gradually and always have the highest temperatures. Vegetation and water keep the temperature low by playing a regulating role.

Figure 13 shows a slight variation in temperature between the vegetation, buildings, and soil classes, which suggests that the regulatory role that vegetation plays on temperature seems to be attenuated by significant urbanization and the urban heat island effect.

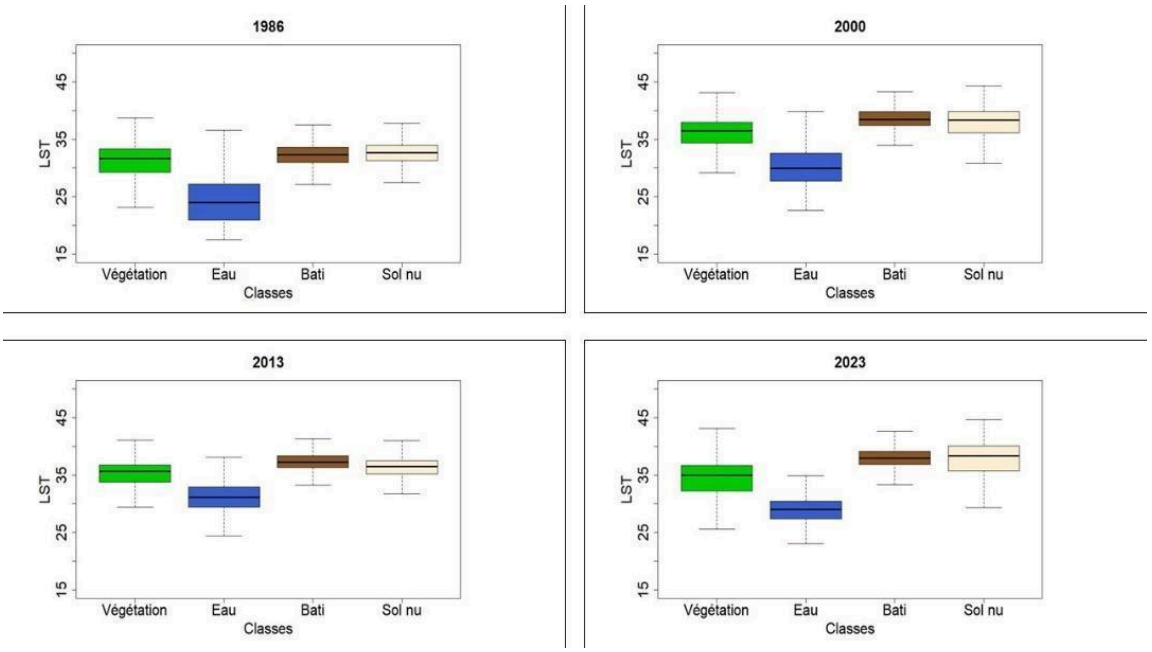

III.6.1.1) Figure 12: Variation of LST values between different land use classes

III.6.2) LST variation in vegetated lands

To analyze the variation of LST in vegetated areas, NDVI maps from 1986 to 2023 were produced (Figure 14). The figure represents the spatial distribution of NDVI. It can be seen that NDVI does not have a great influence on the area.

A slight variation is observed between 1986 and 2000 and a small increase in 2013 before experiencing a decrease in 2023.

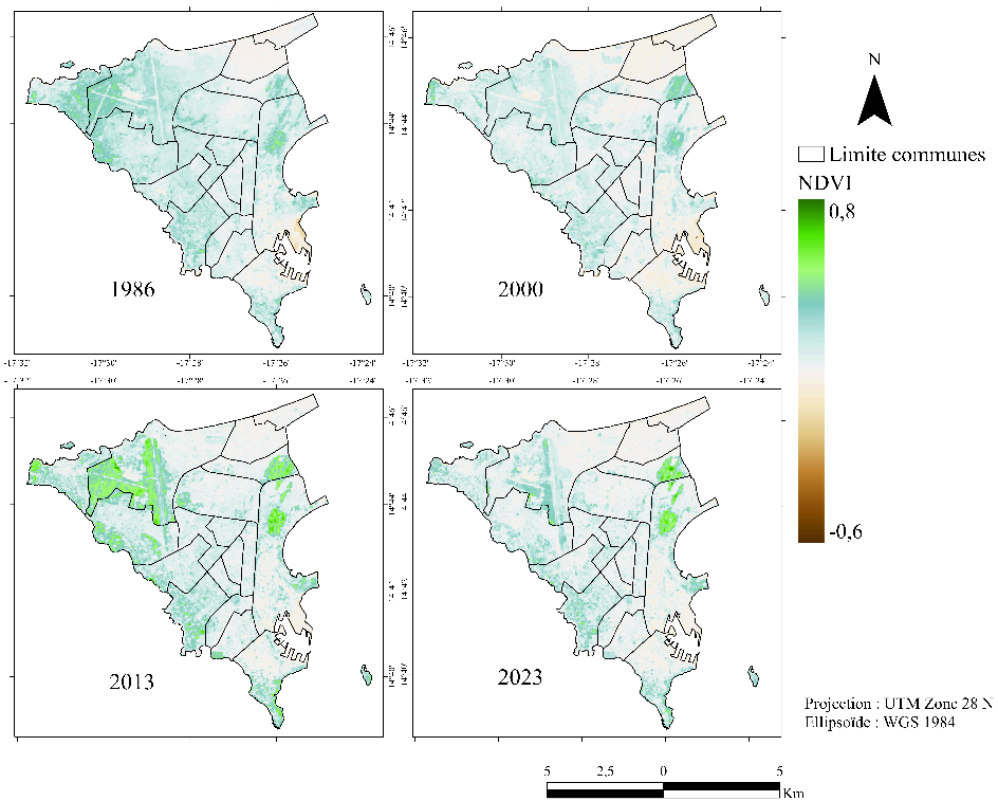

III.6.2.1) Figure 13: NDVI maps for the years 1986, 2000, 2013 and 2023

As documented in the literature, areas with high LST are found to be areas with low vegetation. A negative relationship between LST and NDVI should be observed after correlation and regression analysis which is not the case in the figure. This may be due to the low amount of vegetation in the study area which has little influence on temperature, or the effect of vegetation on the atmosphere is negligible considering the environment of the city of Dakar (Figure 15).

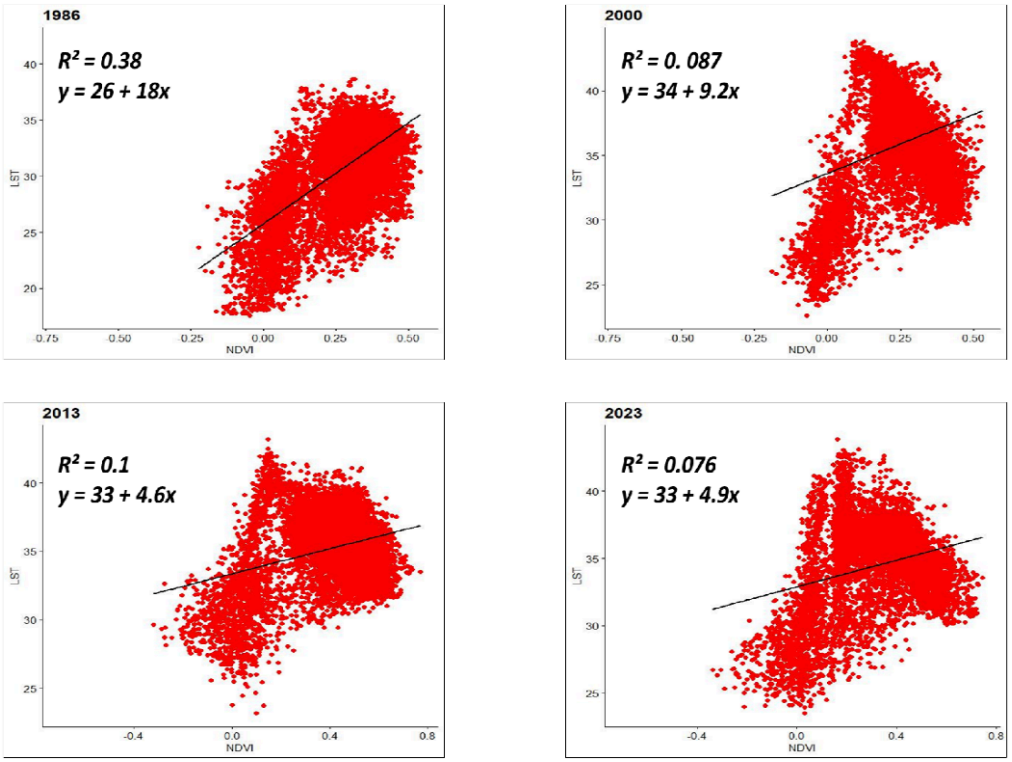

III.6.2.2) Figure 14: Correlation between LST and NDVI for the years 1986, 2000, 2013 and 2023

III.6.3) LST variation in wetlands

To analyze the changes in the water index, NDWI maps from 1986 to 2023 were prepared (Figure 16). The figure showed that the area covered by water was too low over the years, and the figure shows a fairly low NDWI value over the four years.

As with NDVI, the wettest areas should have low temperature and vice versa. Therefore, a negative relationship exists between LST and NDWI as illustrated in Figure 17. The R^2 values are 0.47, 0.47, 0.27 and 0.17 for the years 1984, 2000, 2013 and 2023, respectively.

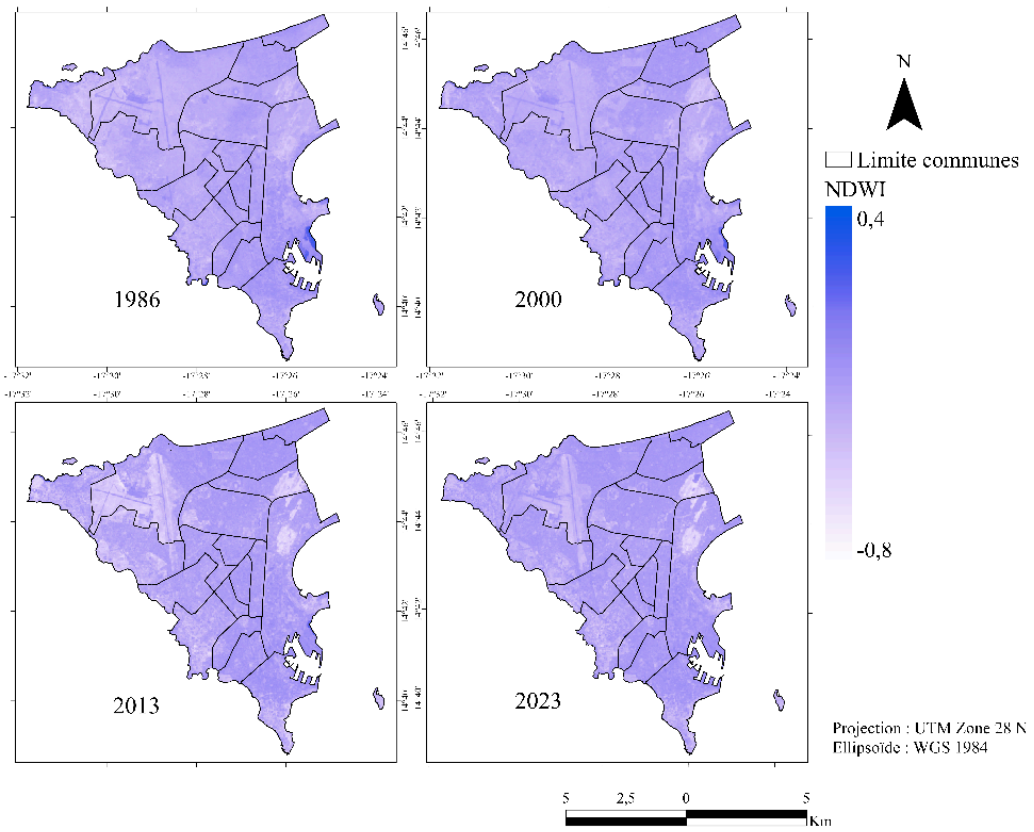

III.6.3.1) Figure 15: NDWI maps for the years 1986, 2000, 2013 and 2023

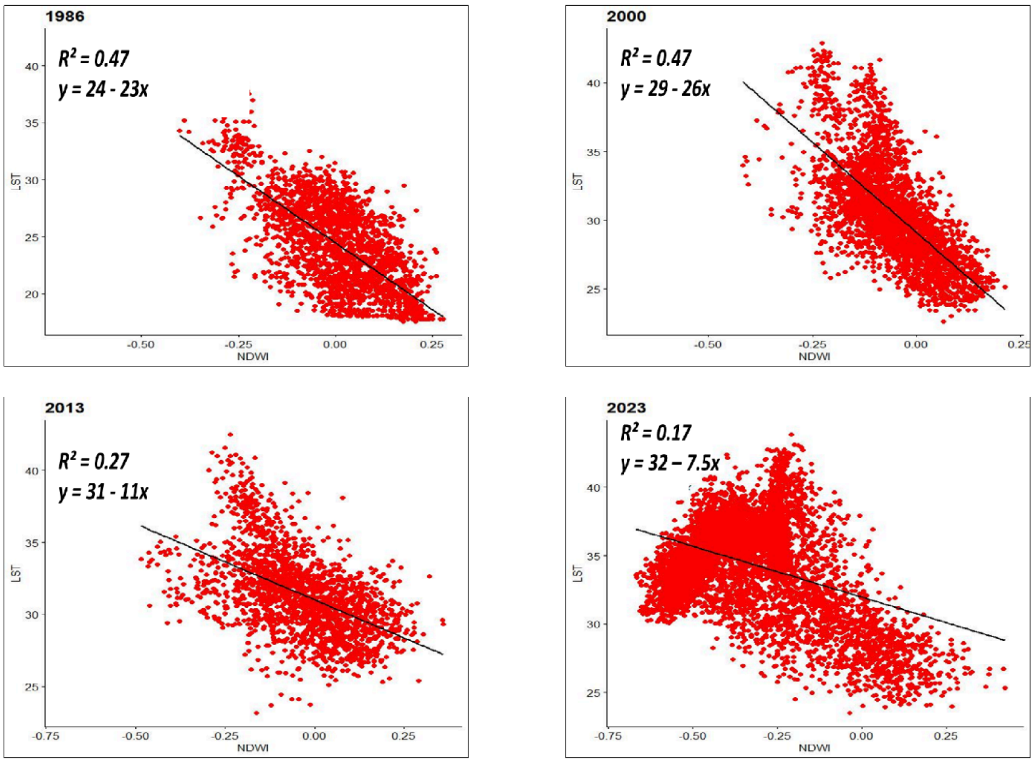

III.6.3.2) Figure 16: Correlation between LST and NDWI for the years 1986, 2000, 2013 and 2023

III.6.4) Variation of LST in built-up areas

To examine the changes in built-up areas, NDBI maps from 1986 to 2023 were prepared. From the analysis, the built-up density is much higher from 2000 onwards. As shown in Figure 18, there is a significant increase in built-up areas between 1986 and 2023. From the regression (Fig. 19) and correlation analysis, we can say that there is a positive relationship between LST and NDBI even though it appears weak from the regression coefficients R^2 (0.0059 for 1986, 0.1 for 2000, 0.061 for 2013 and 0.066 for 2023).

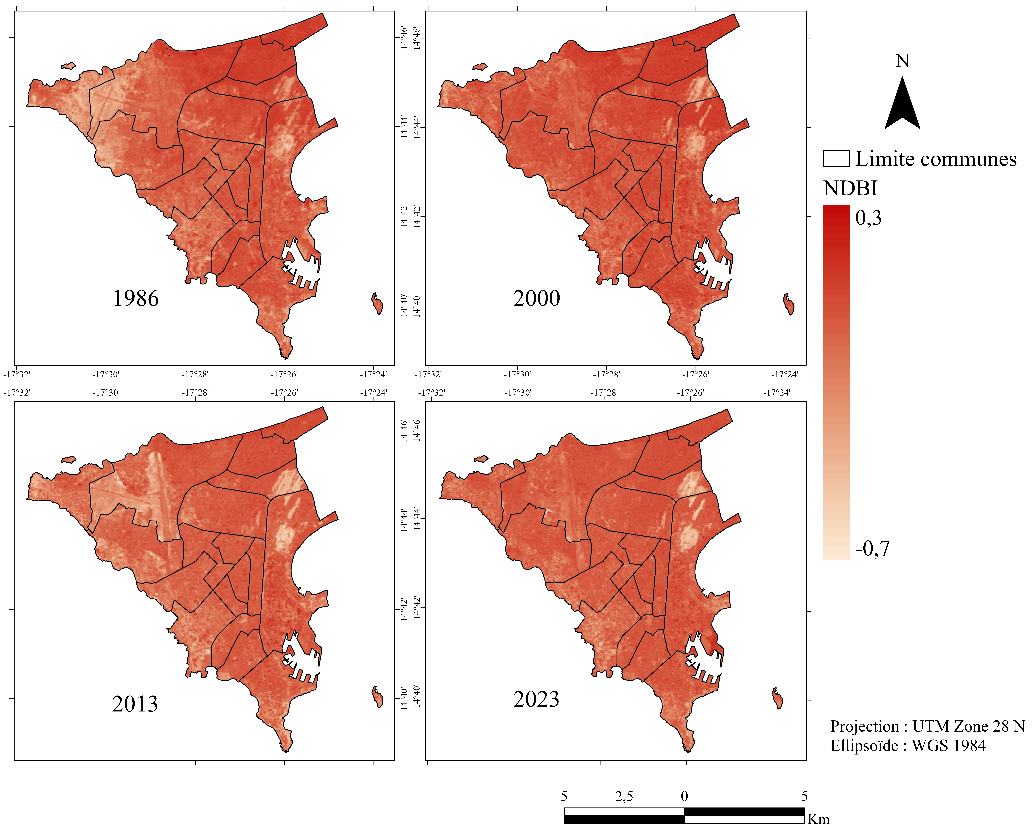

III.6.4.1) Figure 17: NDBI maps for the years 1986, 2000, 2013 and 2023

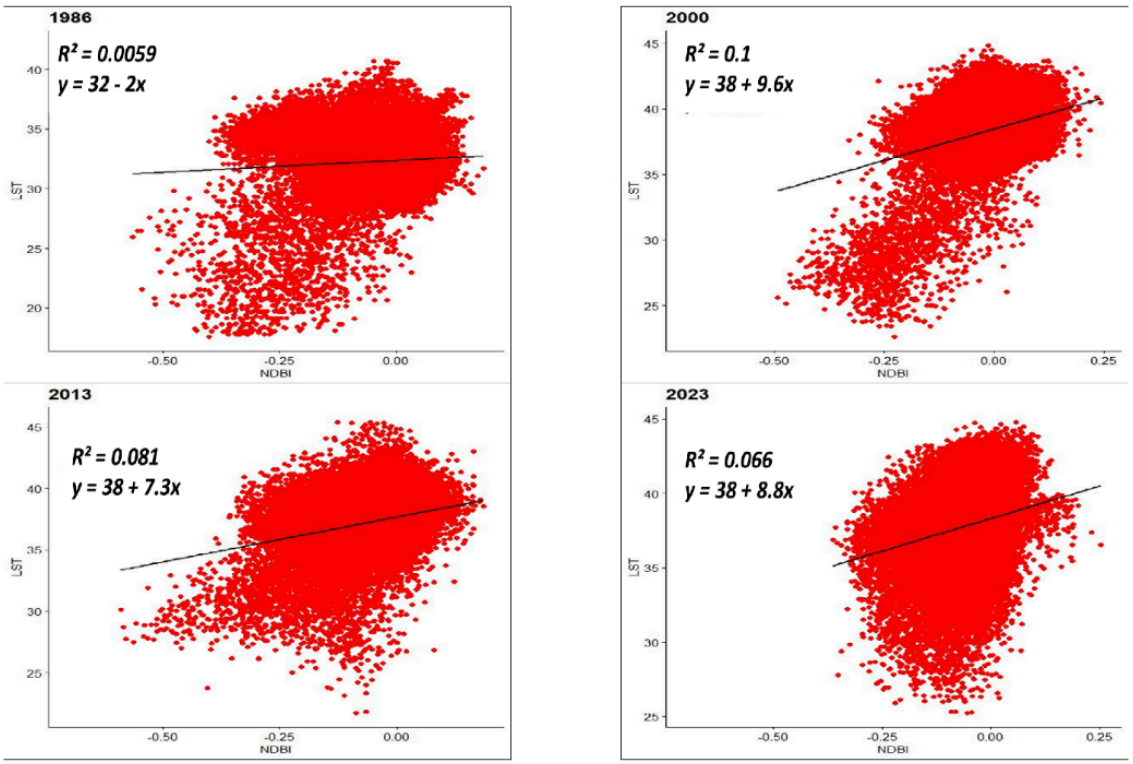

III.6.4.2) Figure 18: Correlation between LSTs and NDBIs for the years 1986, 2000, 2013 and 2023

IV) Discussion

IV.1) Rapid urbanization growth and thermal change in Dakar

Senegal is experiencing rapid urbanization, which is generating uncontrolled land use. The city of Dakar is particularly affected. The increase was significant between 1986 and 2023. Since 2000, the city has experienced a construction boom, including the expansion of the Dakar Autonomous Port and the construction of new road infrastructure, primarily in the southeastern part of the study area.

The study of urban expansion provides crucial information on temperature fluctuations in the city. In 1986, much of the area, particularly in the city center and northeast side, was still undeveloped. As a result, the temperature was not as high even with a small amount of water and vegetation cover, which acted as a regulator. In contrast, in the years 2000, 2013, and 2023, the temperature was too high due to rapid urbanization.

The results of this study showed that the average temperatures of urban areas and bare soils were almost similar. However, this can be explained by the fact that the moisture content of bare soils is too low in the study area. Contrary to the results obtained by other researchers, the results of this study revealed a positive correlation between LST and NDVI, probably due to the low vegetation density in this area and insufficient spatial resolution to distinguish between different types of vegetation cover.

These findings highlight the impact of urban development on local thermal conditions, underscoring the need for integrated and sustainable urban management practices. Adopting sustainable approaches to urban planning is essential to minimize negative impacts on the city's climate. This includes promoting environmentally friendly architecture, developing green spaces, building artificial lakes, and implementing urban policies that aim to balance growth with the conservation of natural resources. Sustainable urban management is crucial to preserving residents' quality of life while maintaining the unique character of Dakar.

IV.2) Limited influence of vegetation on LST

The positive relationship between NDVI and LST indicates that vegetation cover is too low in the city. This result suggests that vegetation, although present, has only a limited influence on surface temperature. This weak influence could be due to reduced plant density, significant water stress, or other environmental factors that limit the effectiveness of vegetation as a heat shield.

IV.3) Advancing research on LST and LU

Conventional approaches to assessing the effects of land-use changes on surface temperature typically involve manually compiling data from a variety of sources, including weather stations, field surveys, and satellite information. These methods can be laborious and require a substantial investment of time and effort. Field surveys will need to be conducted, weather stations established, and data accumulated over specific periods to determine the impact of land-use changes on surface temperature. However, the development of the GEE platform has been of great significance in this area, providing significant benefits in exploring land-use changes and their effects on surface temperature.

V) Conclusion

This study assessed the impact of LU changes on LST in the city of Dakar, from 1986 to 2023, leveraging the power of GEE. Using a classification approach combined with spectral indices, we obtained results thus achieving the objective we had set on the diachronic study of land use from 1986 to 2023. The analysis focused on four classes namely vegetated areas, built-up areas, bare soils and water areas, which shows a significant urban growth and a corresponding decrease in vegetated and wetland areas.

This study also explored the relationship between land surface temperature and different land cover and land use classes. This shows a variation in the temperature of the land surface of the classes over the years (vegetation: 31.67°C in 1986; 31.37°C in 2000; 31.88°C in 2013 and 30.87°C in 2023), (water: 24.02°C in 1986; 24.91°C in 2000; 25.65°C in 2013 and 27.39°C in 2023), (built-up: 32.32°C in 1986; 32.52°C in 2000; 32.48°C in 2013 and 32.50°C in 2023), (bare soil: 33.64°C in 1986; 32.58°C in 2000; 32.38°C in 2013 and 32.92°C in 2023).

The results of correlation analysis between LST and spatial indices like NDVI, NDWI and NDBI did not show a close relationship, which should clearly prove how urbanization affects thermal

environment and water body, vegetation cover and urbanization over time. The study shows a weak positive relationship between LST and NDBI (r^2 = 0.005 in 1986; 0.10 in 2000; 0.081 in 2013 and 0.066 in 2023), a positive relationship between LST and NDVI (r^2 = 0.38 in 1986; 0.087 in 2000; 0.1 in 2013 and 0.076 in 2023) and a negative relationship between LST and NDWI (r^2 = 0.47 in 1986 and 2000; 0.27 in 2013; and 0.17 in 2023). In addition, by statistical analysis, we also found that in built-up areas, the heat island effect is much greater than in other areas.

Finally, remote sensing techniques and the new GEE platform have radically changed the way we access and use geographic data. GEE's extensive geodata library, advanced algorithms, and cloud computing capabilities, including the classification model, allow for easier, faster, and more accessible data analysis, enabling us to conduct a diachronic analysis of land cover and land surface temperature in the city of Dakar over the past 40 years. The results presented here could serve as a theoretical basis for urban planning and decision-making for better future land management to avoid excessive use. To promote thermal comfort in Dakar, tree planting exercises are some of the recommendations made.

VI) Bibliography

(nd). Retrieved from Climates and Travel: https://www.climatsetvoyages.com/climat/senegal/dakar

Anandababu, Purushothaman, & Babu, D. S. (n.d.). Estimation of Land Surface Temperature using LANDSAT 8 Data. IJARIT, 117-185.

Bubun, M., Siba, SS, L'Archiviste, S., Rana, L., & Mukul, M. (2024). Dynamicsspatio-temporal Land use and cover (LUC) changes and their impact on land surface temperature: A case study in New Kolkata, eastern India. ScienceDirect, 2-20.

Gajani, AM (2024). Spatial patterns of urban heat islands and green spaces. Cooling effects in the urban microclimate of Karachje. Urban Climate.

Google Earth Engine. (nd). Retrieved from ee.Classifier.smileGradientTreeBoost: https://developers.google.com/earth-engine/apidocs/ee-classifier-smilegradienttreeboost

Google Earth Engine. (nd). Retrieved from Ee.Classifier.SmileGradientTreeBoost.: https://developers.google.com/earth-engine/apidocs/ee-classifier-smilegradienttreeboost

Jianga, J., & Tiana, G. (2023). Analysis of the impact of land use and land cover changes on land surface temperature using remote sensing. International Society for Environmental Information Sciences, 571-575.

ME Awuh, PO Japhets, MC Officha, AO Okolie, & IC Enete. (2019). Correlation Analysis of the Relationship Between Land Use and Land Cover/Land Surface Temperature in Abuja Municipality, FCT, Nigeria. Journal of Geographic Information System, 44-55.

Mirza, W., & Sajjadb, M. (2022). Exploiting cloud computing and spatial modeling approaches for land surface temperature disparities in response to land cover change: Evidence from Pakistan. Remote Sensing Applications: Society and Environment, 2-19.

Mwangi, PW, Faith, NK, & Peter, KK (2018). Analysis of the relationship between land surface temperature and vegetation and building indices in Upper-Hill, Nairobi. Journal of Geoscience and Environment Protection, 1-16.

Mwangi, PW, Karanja, FN, & Kamau, PK (2018). Analysis of the relationship between land surface temperature and vegetation and built-up indices in Upper-Hill, Nairobi. Journal of Geoscience and Environment Protection, 1-16.

Niladri, D., Prolay, M., Subhasish, S., & Ranajit, G. (2021). Assessment of Land Use/Cover Variation and Its Impact on Land Surface Temperature of Asansol Subdivision. The Egyptian Journal of Remote Sensing and Space Sciences, 2-18.

Pal, S., & Ziaul, S. (2017). Detection of land use and cover changes and land surface temperature in the urban center of English Bazar. ScienceDirect, 125-145.

Ullah, S., Fan, B., & Liu, D. (2019). Modeling the Impact and Risk Assessment of Urbanization on Urban Heat Island and Thermal Comfort Level of Beijing City, China (2005-2020). Sustainability, 2-18.